



# Zinc and silver containing mesoporous bioactive glass nanoparticles for bone regeneration

Parichart NARUPHONTJIRAKUL\*

Biological Engineering Program, Faculty of Engineering,  
King Mongkut's University of Technology Thonburi  
parichart.nar@kmutt.ac.th

Wen-Ta Su

Department of Chemical Engineering and Biotechnology,  
National Taipei University of Technology  
f10549@ntut.edu.tw

## ABSTRACT

Mesoporous bioactive glass nanoparticles (MBGNs) have been widely used to deliver therapeutically active ions as multi-functional nanocarriers for bone regeneration applications. Copper (Cu), strontium (Sr), and zinc (Zn) were successfully incorporated into the MBGNs (60SiO<sub>2</sub>-40CaO) using the microemulsion-assisted sol-gel method and the post-functionalization process. The monodispersed spherical particles with a diameter size range of 110 ± 20 nm (SEM) were stable in the aqueous solution (Zeta potential >-30 mV). Sr, Zn, and Ag were successfully incorporated into the MBGNs without altering their amorphous structure and chemical structure of the particles. The diameter pore ranged from 4.5 to 5.6 nm indicating the mesoporous structure. The surface area increased from 120 (MBGNs) to 128 m<sup>2</sup>g<sup>-1</sup> (doped MBGNs). All MBGNs exhibited *in vitro* bioactivity when immersed in simulated body fluid and showed no cytotoxicity towards MC3T3-E1 pre-osteoblast cells up to the particle concentration at 200 µg/mL. Sr-Zn@MBGNs, Sr-Ag@MBGNs, and Sr-Ag-Zn@MBGNs showed antibacterial activity against *E. coli* and *S. aureus*. The addition of Sr, Zn, and Ag to MBGNPs enhanced their effectiveness in antibacterial activity and bioactivity.

## KEYWORDS

Antibacterial, Bioactivity, Mesoporous bioactive glass nanoparticles, Zinc, Silver

### ACM Reference Format:

Parichart NARUPHONTJIRAKUL and Wen-Ta Su. 2023. Zinc and silver containing mesoporous bioactive glass nanoparticles for bone regeneration. In *2023 10th International Conference on Biomedical and Bioinformatics Engineering (ICBBE 2023)*, November 09–12, 2023, Kyoto, Japan. ACM, New York, NY, USA, 7 pages. <https://doi.org/10.1145/3637732.3637753>

## 1 INTRODUCTION

Bioactive glasses (BGs) are silica-based glasses in which the silica is network former and modified with network formers, network modifiers, and intermediate including alkali metals such as sodium and potassium or alkaline earth metals such as calcium and magnesium [1-3]. The first bioactive glass, 45S5 Bioglass<sup>®</sup>, composed of 46.1

mol% SiO<sub>2</sub> 26.9 mol% CaO 24.4 mol% Na<sub>2</sub>O and 2.5 mol% P<sub>2</sub>O<sub>5</sub>, was developed by Hench in the late 1960s and early 1970s [4]. BGs can form bonds to the host bone tissue without the formation of scar tissues between the implant material and the host tissue in *in vivo* and was easy to melt due to the lower melting point of Na<sub>2</sub>O [4, 5]. BGs have been improved the biocompatible and bioactive properties by incorporating the silica tetrahedron based material with the network modifiers [3]. The therapeutic ions contained within the BGs were released and diffused into the body fluid, leading to the activation of osteoinduction through the expression of genes that promote the formation of new bone [6-8]. BGs have been used in various forms such as granules, microparticles, and nanoparticles. Dense and mesoporous bioactive glass nanoparticles have been intensively interested in using as a nanocarrier for stimulating bone formation. This interest stems from their unique characteristics, such as a large specific surface area, the ability to be taken up by cells, and the capacity to localize and release therapeutic ions or agents in a targeted manner [9-12].

Mesoporous bioactive glass nanoparticles (MBGNs) have increased significant attention in recent years due to their unique properties and potential applications in various fields, including biomedicine, drug delivery, tissue engineering, and regenerative medicine. MBGNs have ordered and interconnected pore structures with diameter pore size ranging from 2 to 50 nm that provide a high surface area and large pore volume, enabling efficient loading and sustained release of therapeutic agents. The large surface area of mesoporous structure allowed efficient interactions with biomolecules and cells, resulting in enhancing their biological activity and cellular interactions such as cell adhesion, proliferation, and differentiation. In addition, therapeutic ions released from MBGNs stimulated osteogenic and angiogenic properties that are particularly useful in bone tissue engineering and repair applications.

The composition of MBGNs was crucial for controlling their biocompatibility, bioactivity, degradation rate, drug delivery capabilities, and surface properties. The composition of MBGNs can be tailored to ensure biocompatibility with specific biological response. Optimizing the composition enables the development of MBGNs that were better suited for specific applications in biomedical engineering and regenerative medicine. The beneficial cations such as calcium (Ca), strontium (Sr), zinc (Zn), copper (Cu), and silver (Ag) have been incorporated into the silica network to perform a sustained release and enhance bioactivity. Ca, an essential component of bone tissue, enhances bioactivity through the release of ions and the formation of a biologically active surface layer. Ca played a role in stimulating osteoblast activity and inhibiting osteoclast activity. Sr, a beneficial trace element, can stimulate bone formation by inducing osteoblast activity and inhibiting osteoclast activity

\*Corresponding Author: Parichart Naruphontjirakul Biological Engineering Program, Faculty of Engineering, King Mongkut's University of Technology Thonburi, Thailand.



This work is licensed under a Creative Commons Attribution International 4.0 License.

ICBBE 2023, November 09–12, 2023, Kyoto, Japan  
© 2023 Copyright held by the owner/author(s).  
ACM ISBN 979-8-4007-0834-3/23/11  
<https://doi.org/10.1145/3637732.3637753>

[13-17]. Zn, an essential trace element, has been shown to have an important role in bone formation both *in vitro* and *in vivo* [18]. It is fundamental for bone cell growth, development, and differentiation [19]. Zn deficiency causes skeletal growth delay and is associated with alterations in bone tissue calcification [20]. Zn also has inherent antibacterial properties. Ag imparted additional antimicrobial properties to MBGNs [21]. The release of Ag from MBGNs provided a sustained antimicrobial effect, inhibited the growth of bacteria, fungi, and other microorganisms, thus preventing infections [22].

MBGNs showed a unique combination of bioactivity, controlled drug delivery, biocompatibility, and tunable biological properties. These properties make them promising candidates for a wide range of biomedical applications. However, the concentration of doped ions and their potential cytotoxicity should be carefully considered. Thus, the aim of this research was to develop multifunctional MBGNs through the combination of bone regeneration and antibacterial properties by incorporating Sr, Zn and Ag into SiO<sub>2</sub>-CaO binary glass system. The composition of MBGNs was modified using Sr, Zn and Ag co-doping to extend the therapeutic effect of MBGNs. The multifunctional of Sr, Zn, and Ag doped MBGNs were synthesized using the microemulsion-assisted sol-gel method. The cationic surfactant (Cetyltrimethylammonium bromide, CTAB) was used to generate the pore pattern. The impact of Sr, Zn, and Ag doped into the 60SiO<sub>2</sub>-40CaO binary glass system on bioactivity and cellular response was investigated.

## 2 MATERIALS AND METHODS

All reagents were from Sigma-Aldrich (St. Louis, MO, USA) unless stated otherwise. The following were used in this study: tetraethyl orthosilicate (TEOS), ethyl acetate, ammonium hydroxide, ethyl alcohol (99.5%), calcium nitrate tetrahydrate (99%), strontium nitrate (99%), zinc nitrate hexahydrate (≥98%), silver nitrate (99%), phosphate buffered saline (PBS), sodium chloride (NaCl), sodium hydrogen carbonate (Na-HCO<sub>3</sub>), potassium chloride (KCl), di-potassium hydrogen phosphate trihydrate (K<sub>2</sub>HPO<sub>4</sub>·3H<sub>2</sub>O), magnesium chloride hexahydrate (MgCl<sub>2</sub>·6H<sub>2</sub>O), hydrochloric acid (HCl), calcium chloride (CaCl<sub>2</sub>), sodium sulfate (Na<sub>2</sub>SO<sub>4</sub>), minimum essential medium eagle alpha (α-MEM, Gibco™, Thermo Fisher Scientific, Waltham, MA USA), fetal bovine serum (FBS, Thermo Fisher Scientific), Antibiotic-Antimycotic (Thermo Fisher Scientific), trypsin-EDTA (Thermo Fisher Scientific), 3-(4,5-dimethylthiazol-2-yl)-2,5-diphenyltetrazolium bromide (MTT, Thermo Fisher Scientific), dimethyl sulfoxide (DMSO), dexamethasone (DEX), β-glycerophosphate, L-ascorbic acid, paraformaldehyde, Alizarin Red S, Mueller-Hinton Agar (MHA, Difco™, Bangkok, Thailand), MC3T3-E1 cells (ATCC® CRL-2593™) was purchased from ATCC (Biomedica, distributor of ATCC).

### 2.1 MBGN preparation

Briefly, 0.5 g of CTAB was dissolved in 26 mL of pre-heated deionized water at 55°C in a 250 mL DURAN® original laboratory bottle at a stirring rate of 500 rpm for 3 minutes. Then, 8 mL of ethyl acetate was added in the mixed solution. 5.6 mL of 2 M ammonium hydroxide solution was added. 2.9 mL of tetraethyl orthosilicate (TEOS) was added and stirred for 30 minutes. Then calcium nitrate tetrahydrate, strontium nitrate, zinc nitrate hexahydrate, and silver

nitrate were weighed (with the nominal ratio as shown in Table 1) and added. After 4 h of reaction, the colloidal particles were collected using centrifugation at 7380 rpm for 30 minutes. The particles were washed with DI water two times and ethanol two times before drying at 60 °C overnight and calcination at 680°C with a heating rate of 2°C/minute for 4 h.

### 2.2 MBGN characterization

To investigate the size and morphology of the particles, dynamic light scattering (DLS) and emission scanning electron microscopy (SEM, JEOL, JSM-6610 LV, Japan) operating at 20 kV were used. To confirm the elemental components of the synthesised MBGNs, X-ray fluorescence (XRF: Fisher/XUV773) with X-ray generators in at 20 kV operating in a vacuum were used. To analyze texture analysis, specific surface area analyzer (BET, BELSORP-mini II, BEL, Japan) was used. BET multipoint analysis was used to calculate the specific surface area, as the material being used is mesoporous, the P/Po data points were selected from the range 0.05-0.35. To identify the functional groups and crystalline structure of the MBGNs, Fourier transform infrared spectroscopy (FTIR; Thermo Scientific Nicolet iS5, USA) in attenuated total reflection (ATR) mode at a wavenumber ranging from 4000 to 400 cm<sup>-1</sup> at a scan speed 32 scan/min with a resolution of 4 cm<sup>-1</sup> and X-ray Diffractometer (XRD, Bruker AXS Model D8 Advance, Germany) using Cu Kα radiation (1.5406 Å) at 40KV/40mA. Data were collected in the 10–70° 2θ range with a step size of 0.02° and a dwell time of 0.5 s were used, respectively.

### 2.3 Bioactivity Assessment

75 mg of particles were incubated in the 50 ml of SBF solution at pH 7.4 37 °C shaking at 120 rpm for 21 days. The morphological structures and composition of soaked particles were detected using SEM (JEOL, JSM-6610 LV, Japan) and EDS-SEM (OXFORD, INCAx-act, UK), respectively.

### 2.4 Cytotoxicity Assessment

To evaluate the cytotoxicity effect of scaffolds on cell viability, MTT colorimetric assay (Thermo Fisher Scientific) was used according to the manufacturer's instructions. MC3T3-E1 cells (ATCC® CRL-2593™) were seeded in the flat-bottomed 96-well plates at the cell concentration 5×10<sup>3</sup> cells/well. The MC3T3-E1 were treated with different concentrations of particles ranging from 0 to 1 mg/mL: 0, 1, 10, 50, 100, 200, 250, 500, 750, and 1000 µg/mL for 24 h. Cell viability was determined using the MTT colorimetric assay based on the conversion of 3-(4,5-dimethylthiazol-2-yl)-2,5-diphenyltetrazolium bromide (MTT) into formazan. The formazan is soluble in dimethyl sulfoxide (DMSO) and the concentration of soluble formazan was determined using a microplate reader (Infinite®200 Tecan, Austria) at 570 nm. The relative cell viability (% viability compared to untreated cells: control) was calculated as mean value ± standard error of the mean (n = 6).

### 2.5 Antibacterial activity

Antibacterial activity was determined using the disc diffusion method against *Staphylococcus aureus* ATCC 6538 and *Escherichia coli* ATCC 8739 (obtained from the Department of Microbiology,

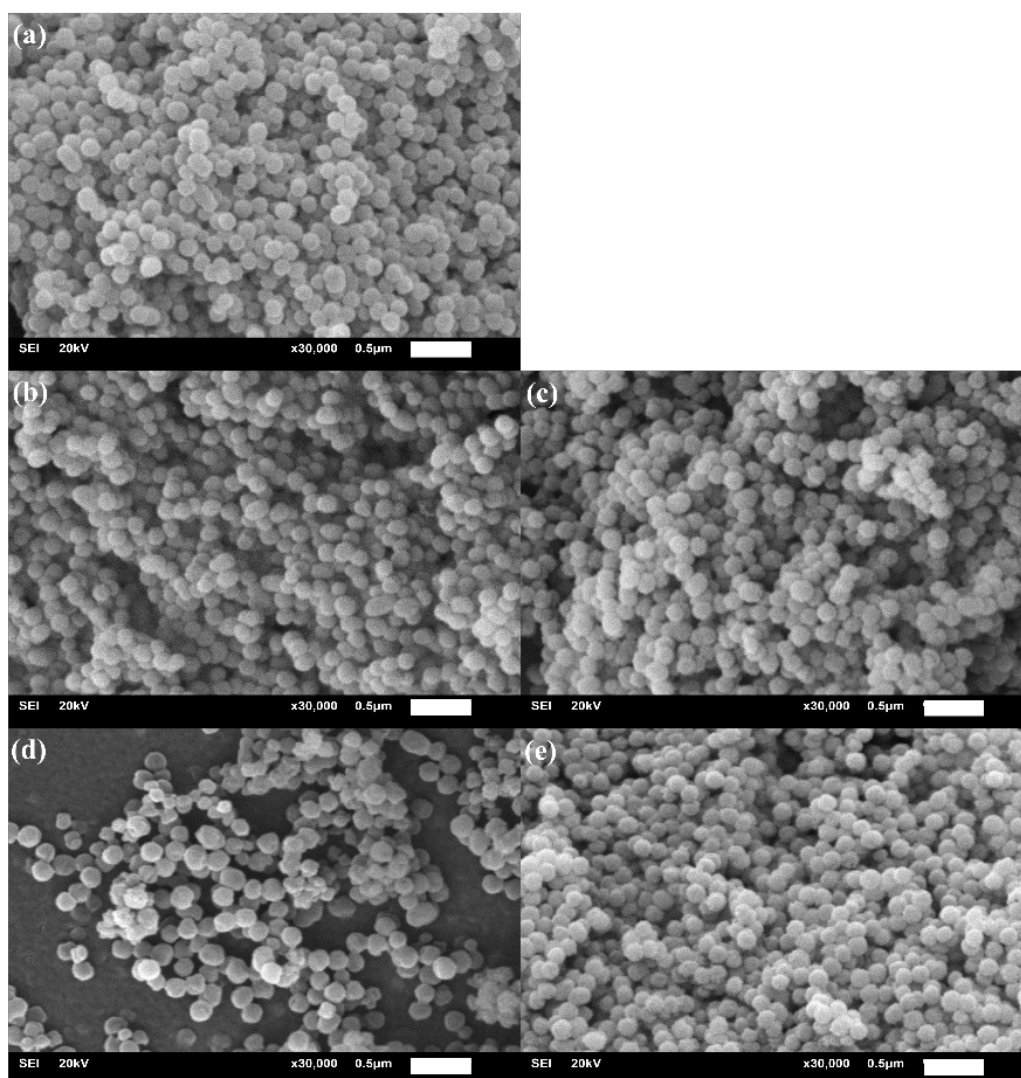


**Figure 1:** SEM images of (a) MBGNs, (b) Sr@MBGNs, (c) Sr-Zn@MBGNs, (d) Sr-Ag@MBGNs, and (e) Sr-Ag-Zn@MBGNs. JEOL, JSM-6610 LV: Operate at 20 kV and 30 kX. Scale bar = 0.5  $\mu\text{m}$ .

**Table 1:** Compositions of MBGNPs (nominal ratio)

	% mol				
	SiO <sub>2</sub>	CaO	SrO	ZnO	Ag <sub>2</sub> O
MBGNs	60	40			
Sr@MBGNs	60	20	20		
Sr-Zn@MBGNs	60	20	14	6	
Sr-Ag@MBGNs	60	20	14	6	
Sr-Ag-Zn@MBGNs	60	20	14	3	3

Faculty of Science, King Mongkut's University of Technology Thonburi, Thailand). *E. coli* and *S. aureus* isolates were grown overnight on Mueller Hinton Agar (MHA) at 37°C and streaked onto the dried surface of an MHA plate. Twenty microliters of MBGNs were

dropped onto 6-mm-diameter Whatman<sup>®</sup> antibiotic assay discs and placed onto the MHA plates. The halo zone was imaged using Gel Documentation model Syngene Gene Genius after incubation at 37°C for 18 h.

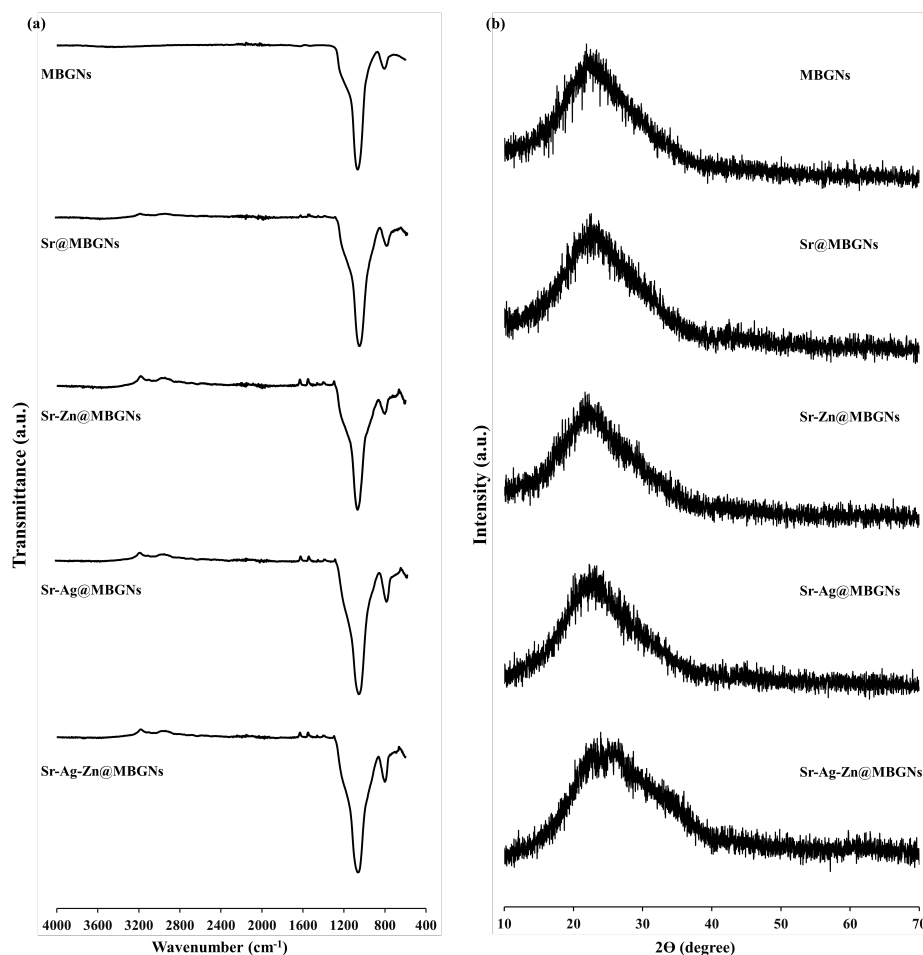


Figure 2: (a) FTIR and (b) XRD spectra of MBGNs, Sr@MBGNs, Sr-Zn@MBGNs, Sr-Ag@MBGNs, and Sr-Ag-Zn@MBGNs.

Table 2: Size and Zeta Potential of MBGNs

	DLS Size (nm)	PDI	Zeta Potential (mV)
MBGNs	158.42 ± 5.56	0.23 ± 0.02	-36.87 ± 1.07
Sr@MBGNs	177.60 ± 8.75	0.19 ± 0.01	-33.60 ± 0.56
Sr-Zn@MBGNs	180.80 ± 0.79	0.17 ± 0.01	-43.90 ± 0.69
Sr-Ag@MBGNs	156.60 ± 4.55	0.20 ± 0.03	34.67 ± 0.57
Sr-Ag-Zn@MBGNs	185.67 ± 0.67	0.11 ± 0.00	-47.63 ± 1.14

## 2.6 Statistical Analysis

All reported values in this study are mean (SD). Statistical analyses were performed by one-way analysis of variance (ANOVA) in Minitab with the appropriate post hoc comparison test (Tukey's test). A *p*-value < 0.05 was considered significant.

## 3 RESULTS AND DISCUSSIONS

The monodispersed MBGNs with the particle size range of 160 ± 20 nm were successfully synthesised through the microemulsion-assisted sol-gel process using 2M ammonium hydroxide as the base

catalyst to control hydrolysis and poly-condensation reactions that controlled the size of the particles (Table 2). Therapeutic cations including Sr, Zn, and Ag were doped into MBGNs (60SiO<sub>2</sub>-40CaO) through the calcination process at 700 °C for 4 hours. The unreacted precursors were decomposed and eliminated through heat treatment process. The spherical shape and uniformity within the range of 110 ± 20 nm were observed using SEM (ImageJ software *n* = 50), as shown in Figure 1.

The elemental composition of MBGNs using XRF confirmed that beneficial cations Sr, Zn, and Ag were successfully incorporated into

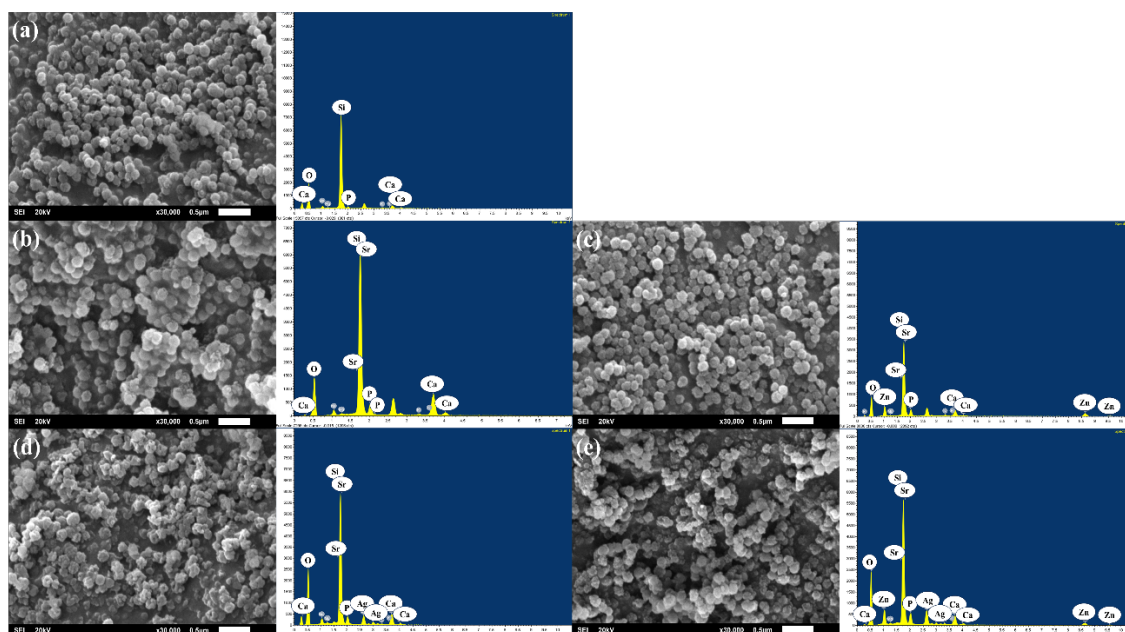


**Figure 3:** SEM images of (a) MBGNs, (b) Sr@MBGNs, (c) Sr-Zn@MBGNs, (d) Sr-Ag@MBGNs, and (e) Sr-Ag-Zn@MBGNs after immersion in SBF for 21 days. JEOL, JSM-6610 LV: Operate at 20 kV and 30 kX. Scale bar = 0.5  $\mu\text{m}$ .

**Table 3: Elemental composition of MBGNs**

	SiO <sub>2</sub>	CaO	% mol		
			SrO	ZnO	Ag <sub>2</sub> O
MBGNs	73.81	26.19			
Sr@MBGNs	70.14	15.13	14.73		
Sr-Zn@MBGNs	59.38	5.11	4.54	30.97	
Sr-Ag@MBGNs	58.72	5.45	6.57		29.26
Sr-Ag-Zn@MBGNs	59.35	5.94	5.38	15.18	14.15

the glass network as shown in Table 3. These results indicated that the composition of MBNGs (60SiO<sub>2</sub>-40CaO) can be modified with Sr, Zn, and Ag using the microemulsion-assisted sol-gel process. Interestingly, the amount of Ca and Sr were significantly reduced after Zn and Ag were incorporated indicating that Zn and Ag have high binding efficiency to the silica network compared to Ca and Sr [23]. The FTIR spectra indicated the identical chemical bonding of silica network in the MBGNs (Figure 2 (a)). The transmittance peak at 800 cm<sup>-1</sup> and 1000-1200 cm<sup>-1</sup> indicated the symmetric Si-O-Si stretching and the asymmetric Si-O-Si stretching [24]. Doping with different amounts of Sr, Zn, and Ag did not significantly change the chemical structure of the particles. The XRD spectra of synthesised MBGNs represented the broad halo band at  $2\theta \sim 20\text{-}30^\circ$  that related to amorphous structure of MBGNs, indicating that Sr, Zn, and Ag were doped to MBGNs whilst maintaining the amorphous structure (Figure 2 (b)).

The textural properties of MBGNs were shown in Table 4. The diameter pore was comparable for MBGNs and doped MBGNs, range from 4.5 to 5.6 nm. The surface area, pore volume, and pore

diameter of doped MBGNs were comparable to that of non-doped MBGNs. These results indicated that the incorporation of Sr, Zn, and Ag did not significantly alter the physicochemical properties of MBGNs including chemical bonding of silica network, amorphous nature, specific surface area, pore volume, and pore diameter. The *in vitro* biomineralization of particles was studied by immersing them in the simulated body fluid (SBF) solution for 21 days and imaging them using SEM and EDS-SEM (Figure 3). An apatite layer (cauliflower-like) on the surface of the particles was formed after soaking in the SBF solution for 21 days. This apatite formation facilitated the bone cell growth [25]. Moreover, the EDS-SEM results confirmed Ca and P signal on the surface of the particles. The Sr, Zn, and Ag remained inside the particles, suggesting that Sr, Zn, and Ag performed the sustained release over 21 days of incubation.

The effect of MBGNs on *In vitro* cell viability of MC3T3-E1 was investigated using MTT assay (Figure 4 (a)). The cell viability of MC3T3-E1 treated with Sr@MBGNs statistically significantly increased at the concentration  $\geq 250 \mu\text{g/mL}$  compared to the cells treated with alternative particles at equivalent concentration. The

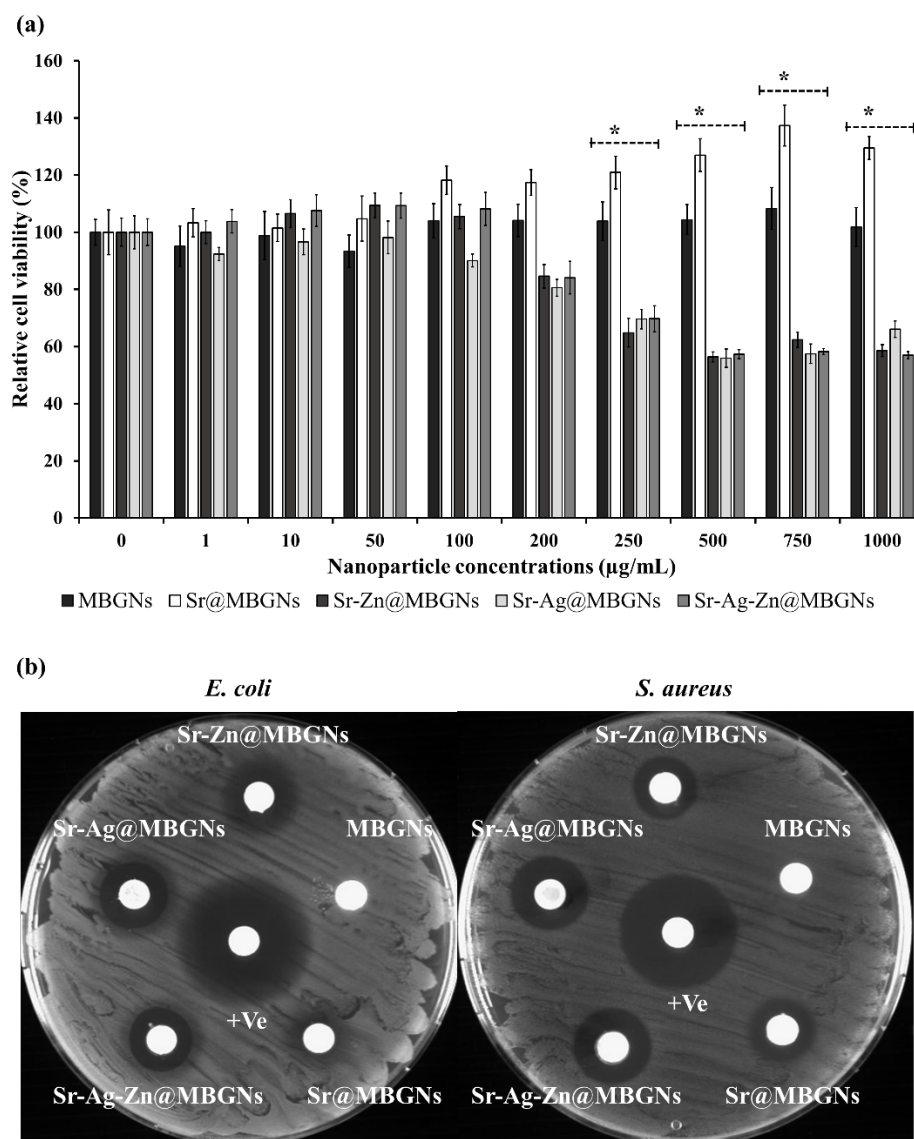


Figure 4: (a) Effect of MBGNs, Sr@MBGNs, Sr-Zn@MBGNs, Sr-Ag@MBGNs, and Sr-Ag-Zn@MBGNs on MC3T3-E1 cell viability after 24 h of incubation ( $n = 6$  per group). (\*) indicates a statistically significant difference compared to controls (untreated cells) ( $p < 0.05$ ). (b) Antibacterial diffusion "halo" results against *E. coli* and *S. aureus*. Positive control (+ve) was Penicillin/Streptomycin (Pen/Strep).

Table 4: Size and Zeta Potential of MBGNs

	BET Surface Area ( $a_{s,BET}$ ) [ $\text{m}^2 \text{g}^{-1}$ ]	Total pore volume [ $\text{cm}^3 \text{g}^{-1}$ ]	Average pore diameter [nm]
MBGNs	120.64	0.31	4.52
Sr@MBGNs	128.58	0.31	5.53
Sr-Zn@MBGNs	127.66	0.37	5.37
Sr-Ag@MBGNs	124.30	0.34	5.61
Sr-Ag-Zn@MBGNs	124.32	0.33	5.50

cell viability less than 70% was considered a cytotoxic effect. Adding Ag and Zn into MBGNs caused toxic to the cell (at the concentration  $\geq 250 \mu\text{g/mL}$ ). The antibacterial effect of MBGNs was investigated against *E. Coli* and *S. aureus* using a disc diffusion method (Figure 4 (b)). There was no inhibition zone formation of MBGNs. Interestingly, Sr@MBGNs, Sr-Zn@MBGNs, Sr-Ag@MBGNs, and Sr-Ag-Zn@MBGNs had antimicrobial properties with wide range of activity against the Gram-positive (*S. aureus*) and Gram-negative (*E. coli*) bacteria. The preliminary results indicated that the bacteria growth was strongly inhibited by Zn and Ag containing MBGNs associated with the release of Zn and Ag ions [26]. The specific effects of Zn and Ag depended on their concentration. Thus, the release profile of Zn and Ag from particles will be investigated in future.

#### 4 CONCLUSION

These preliminary results indicated that Zn and Ag were successfully incorporated into the MBGNs while maintaining the physicochemical properties of MBGNs. The monodispersed MBGNs with the diameter size range  $110 \pm 20 \text{ nm}$  were stable in an aqueous solution. SEM images confirmed the spherical morphology of all the synthesized particles. BET analysis confirmed the mesoporous structure (2-50nm). Doping Zn and Ag in the MBGNs did not significantly alter the specific surface area, pore size, pore volume, and amorphous nature. MBGNs, Sr@MBGNs, Sr-Zn@MBGNs, Sr-Ag@MBGNs, and Sr-Ag-Zn@MBGNs had no cytotoxicity effect on pre-osteoblast cells up to the particle concentration of  $250 \mu\text{g/mL}$  and had the ability to form the apatite layer on the particle surface after soaking in the SBF solution. Sr-Zn@MBGNs, Sr-Ag@MBGNs, and Sr-Ag-Zn@MBGNs exhibited antibacterial effect against both Gram-positive and Gram-negative bacteria. Taken together, Zn and Ag containing MBGNs showed promising features for biomedical applications.

#### ACKNOWLEDGMENTS

This research project was supported by the NTUT-KMUTT Joint Research Program, King Mongkut's University of Technology Thonburi and "Office of the Permanent Secretary, Ministry of Higher Education, Science, Research and Innovation" grant number "RGNS 64-098.

#### REFERENCES

- [1] Jones JR. Review of bioactive glass: From Hench to hybrids. *Acta Biomaterialia*. 2013;9:4457-86.
- [2] El-Ghannam A. Bone reconstruction: from bioceramics to tissue engineering. *Expert Review of Medical Devices*. 2005;2:87-101.
- [3] Rabiee SM, Nazparvar N, Azizian M, Vashae D, Tayebi L. Effect of ion substitution on properties of bioactive glasses: A review. *Ceramics International*. 2015;41:7241-51.
- [4] Hench LL. The story of Bioglass. *Journal of materials science Materials in medicine*. 2006;17:967-78.
- [5] Hench LL, Splinter RJ, Allen WC, Greenlee TK. Bonding mechanisms at the interface of ceramic prosthetic materials. *Journal of Biomedical Materials Research*. 1971;5:117-41.
- [6] Jones JR. 3 - Bioactive ceramics and glasses. In: Boccaccini AR, Gough JE, editors. *Tissue Engineering Using Ceramics and Polymers*: Woodhead Publishing; 2007. p. 52-71.
- [7] Xynos ID, Edgar AJ, Buttery LD, Hench LL, Polak JM. Gene-expression profiling of human osteoblasts following treatment with the ionic products of Bioglass®45S5 dissolution. *Journal of Biomedical Materials Research: An Official Journal of The Society for Biomaterials, The Japanese Society for Biomaterials, and The Australian Society for Biomaterials and the Korean Society for Biomaterials*. 2001;55:151-7.
- [8] Jell G, Stevens M. Gene activation by bioactive glasses. *Journal of Materials Science: Materials in Medicine*. 2006;17:997-1002.
- [9] Naruphontjirakul P, Porter AE, Jones JR. In vitro osteogenesis by intracellular uptake of strontium containing bioactive glass nanoparticles. *Acta Biomaterialia*. 2018;66:67-80.
- [10] Naruphontjirakul P, Tsigkou O, Li S, Porter AE, Jones JR. Human mesenchymal stem cells differentiate into an osteogenic lineage in presence of strontium containing bioactive glass nanoparticles. *Acta Biomaterialia*. 2019;90:373-92.
- [11] Pinna A, Torki Baghbaderani M, Vigil Hernández V, Naruphontjirakul P, Li S, McFarlane T, et al. Nanoceria provides antioxidant and osteogenic properties to mesoporous silica nanoparticles for osteoporosis treatment. *Acta Biomaterialia*. 2021;122:365-76.
- [12] Chen L, Zhou X, He C. Mesoporous silica nanoparticles for tissue-engineering applications. *WIREs Nanomedicine and Nanobiotechnology*. 2019;11:e1573.
- [13] Gentleman E, Fredholm YC, Jell G, Lotfibakhshaei N, O'Donnell MD, Hill RG, et al. The effects of strontium-substituted bioactive glasses on osteoblasts and osteoclasts in vitro. *Biomaterials*. 2010;31:3949-56.
- [14] Baron R, Tsouderos Y. In vitro effects of S12911-2 on osteoclast function and bone marrow macrophage differentiation. *European Journal of Pharmacology*. 2002;450:11-7.
- [15] Caverzasio J. Strontium ranelate promotes osteoblastic cell replication through at least two different mechanisms. *Bone*. 2008;42:1131-6.
- [16] Brennan TC, Rybchyn MS, Green W, Atwa S, Conigrave AD, Mason RS. Osteoblasts play key roles in the mechanisms of action of strontium ranelate. *British journal of pharmacology*. 2009;157:1291-300.
- [17] Yamaguchi T. The calcium-sensing receptor in bone. *J Bone Miner Metab*. 2008;26:301-11.
- [18] Hadley KB, Newman SM, Hunt JR. Dietary zinc reduces osteoclast resorption activities and increases markers of osteoblast differentiation, matrix maturation, and mineralization in the long bones of growing rats. *Journal of Nutritional Biochemistry*. 2010;21:297-303.
- [19] Yamaguchi M, Oishi H, Suketa Y. Stimulatory effect of zinc on bone formation in tissue culture. *Biochemical Pharmacology*. 1987;36:4007-12.
- [20] Holloway WR, Collier FM, Herbst RE, Hodge JM, Nicholson GC. Osteoblast-mediated effects on zinc on isolated rat osteoclasts: inhibition of bone resorption and enhancement of osteoclast number. *Bone*. 1996;19:137-42.
- [21] Bano S, Akhtar M, Yasir M, Salman Maqbool M, Niaz A, Wadood A, et al. Synthesis and characterization of silver-strontium (Ag-Sr)-doped mesoporous bioactive glass nanoparticles. *Gels*. 2021;7:34.
- [22] Zheng K, Balasubramanian P, Paterson TE, Stein R, MacNeil S, Fiorilli S, et al. Ag modified mesoporous bioactive glass nanoparticles for enhanced antibacterial activity in 3D infected skin model. *Materials Science and Engineering: C*. 2019;103:109764.
- [23] Naruphontjirakul P, Kanchanadumkerng P, Ruenraroengsak P. Multifunctional Zn and Ag co-doped bioactive glass nanoparticles for bone therapeutic and regeneration. *Scientific Reports*. 2023;13:6775.
- [24] Jones JR, Sepulveda P, Hench LL. Dose-dependent behavior of bioactive glass dissolution. *Journal of Biomedical Materials Research: An Official Journal of The Society for Biomaterials, The Japanese Society for Biomaterials, and The Australian Society for Biomaterials and the Korean Society for Biomaterials*. 2001;58:720-6.
- [25] Kong CH, Steffi C, Shi Z, Wang W. Development of mesoporous bioactive glass nanoparticles and its use in bone tissue engineering. *Journal of Biomedical Materials Research Part B: Applied Biomaterials*. 2018;106:2878-87.
- [26] Neščáková Z, Zheng K, Liverani L, Nawaz Q, Galusková D, Kaňková H, et al. Multifunctional zinc ion doped sol-gel derived mesoporous bioactive glass nanoparticles for biomedical applications. *Bioactive materials*. 2019;4:312-21.